JMEPEG (2012) 21:1133–1140
DOI: 10.1007/s11665-011-0015-0

1059-9495/$19.00

Inverse Identification of the Dynamic Recrystallization Parameters for AZ31 Magnesium Alloy Using BP Neural Network

Yan Lou, Wenhua Wu, and Luoxing Li

(Submitted February 24, 2011; in revised form June 20, 2011)

The effect of the dynamic recrystallization (DRX) parameters are of prime importance to improve the accuracy of the numerical simulation of hot forming processes for metals. However, it is difficult to determine the values of DRX parameters from experiments because of the influence of various factors, such as temperature, etc. In the present study, the DRX parameters for AZ31 magnesium alloy are identified by using the method of inverse analysis based on measured stress, BP neural network algorithm, genetic algorithm (GA), orthogonal experiment, and numerical simulation. Then, by applying the identified parameters in finite element analysis, the comparison between the numerically calculated and the experimental results is made to verify the correctness of the method. The results show that the numerically calculated stress, strain, recrystallized fraction, and average grain size valus are in good agreement with the experimental ones. These results demonstrate that the method of inverse analysis is a feasible and an effective tool for determination of the AZ31 DRX parameters.

Keywords AZ31 magnesium alloy, BP neural network, dynamic recrystallization (DRX) parameters, genetic algorithm (GA), inverse method

1. Introduction

AZ31 magnesium alloy is one of the lightest metals being used for structural application. It is considered a possible alternative to steel and aluminum in automotive and aero industries to satisfy the lightweight requirement. AZ31 magnesium is a low stacking fault energy alloy. Dynamic recrystallization (DRX) is a frequent occurrence in hot deformation processes (Ref 1, 2). During DRX, the microstructure varies greatly, and affects the final properties of the component. Therefore, it is very important to predict and control of the microstructure evolution during DRX. Up to now, several DRX mechanisms of magnesium alloys at different temperatures have been proposed (Ref 3-6). Different DRX and deformation mechanisms were operative at different temperature regions. At low temperatures, twining plays an important role in DRX. At intermediate temperatures, continuous DRX associated with cross-slip occurs. At high temperatures, conventional DRX with self-diffusion occurs.

However, owing to the complexity of DRX process and the limitation of experimental method, it is difficult to describe the DRX process accurately through theoretical or experimental approach. Consequently, how to input nucleation information is critical to modeling and simulation of DRX. Various methods have been proposed to simulate DRX and microstructure evolution, such as Monte Carlo (MC) and cellular automation (CA). Compared with MC, CA model is more veridical and flexible in simulating the DRX process (Ref 7), e.g., it enables quantitative simulation of stored energy-driven migration of boundary (Ref 8), and its time step is more easily mapped to real time (Ref 9). Therefore, this method has been attracting greater attention in recent years. The CA simulations mainly focused on the effect of deformation temperature, strain rate, and initial grain size on DRX.

Dislocation density plays a very significant role in nucleation and microstructure evolution of DRX during hot deformation processing. Therefore, most of the present CA simulations are based on dislocation evolution models (Ref 10-13). Many models are developed to describe the evolution of dislocation density (Ref 10, 11) in primary grains and R-grains, nucleation (Ref 12, 14) and grain growth (Ref 13) during DRX. For a specific CA model of DRX, accurate estimation of the model parameters is an essential prerequisite for assessing the model. However, it is difficult to determine the values of CA model of DRX parameters from experiments because of the influence of various factors, such as temperature, etc. Fortunately, in recent years, the development of the method of inverse analysis based on the field measurements has made rapid strides, and this method has been applied successfully to solve many complex engineering problems (Ref 15-20). The essence of the method of inverse analysis is the realization of optimization techniques. Previous attempts at solution of the inverse problem have involved the use of statistical methods, such as regression analysis with application of relevant transform, for fitting curves to the available experimental data (Ref 21). While such techniques are useful for identifying

Yan Lou and **Wenhua Wu**, College of Mechatronics and Control Engineering, Shenzhen University, Shenzhen 518060 Guangdong, People's Republic of China; and **Luoxing Li,** State Key Laboratory of Advanced Design and Manufacture for Vehicle Body, Hunan University, Changsha 410082, People's Republic of China. Contact e-mail: susanlou121@163.com.

general trends in process inputs and outputs, they are subject to a number of disadvantages. Over the past few years, the interest in artificial neural networks has grown sharply for the more effective application of method of inverse analysis in complex problems (Ref 21). In the field of engineering science and computational mechanics, the research and applications of neural networks are being used very extensively and found to be successful. The BP network is one of the main types being applied to engineering. The related studies concern almost all topics of engineering science and mechanics (Ref 21-24), such as structural identification, parameter and transfer coefficient estimation, equation solver, identification of material characterization, and fault diagnoses, etc.

In the study, the DRX parameters for AZ31 magnesium alloy are identified using the method of inverse analysis based on measured stresses, BP neural network algorithm, genetic algorithm (GA), orthogonal experiment, and numerical simulation. Then, the experimental and numerically calculated stresses based on the identified parameters at various strains are compared to verify the feasibility of the method for determination of the DRX parameters.

2. CA Model of DRX

2.1 Model Assumption

To simplify the simulation process, two assumptions are employed in the model (Ref 25, 26):

(1) The dislocation density is homogeneous in primary grains, and it increases with strain; then, DRX will occur when the dislocation density exceeds the critical value. The initial dislocation density is zero in the new R-grains, and it increases with strain.
(2) During DRX, nucleation initially takes place on primary grain boundaries. Until primary grain boundaries are used up, the nucleation will take place on R-grain boundaries.

2.2 Theoretical Model of DRX

2.2.1 Modeling of Dislocation Evolution. The dislocation evolution model describes the effect of work hardening and dynamic recovery on dislocation density. For both primary grains and R-grains, the variation of dislocation density is calculated by the model proposed by String (Ref 10):

$$\frac{d\rho}{d\varepsilon} = h - r\rho \qquad \text{(Eq 1)}$$

where h and r are the parameters representing work hardening and dynamic recovery, respectively.

$$h = h_0\dot{\varepsilon}\,\exp\left(\frac{Q}{RT}\right), \quad r = r_0\dot{\varepsilon}^{-1}\,\exp\left(\frac{-Q}{RT}\right),$$

where h_0 and r_0 are the parameters representing the initial work hardening and the initial dynamic recovery, respectively. Q is the activation energy. R is the ideal gas constant.

Moreover, the flow stress is typically calculated from the value of dislocation density (Ref 11):

$$\sigma = \alpha\mu b\sqrt{\rho} \qquad \text{(Eq 2)}$$

where α is a dislocation interaction term which equals 0.5-1.0 for most metals; μ is the shear modulus; and b is the magnitude of the Burgers vector.

2.2.2 Modeling of Nucleation. In the CA model, it is assumed that deformation is under the isothermal temperature and same strain rate condition. Nucleation is triggered while the dislocation density of the matrix reaches a critical value ρ_c. The critical density depends on the deformation conditions as (Ref 12):

$$\rho_c = \left(\frac{20\gamma_m\dot{\varepsilon}}{3blm\tau^2}\right)^{1/3} \qquad \text{(Eq 3)}$$

where γ_m is the boundary energy for a high angle boundary; m is the grain boundary mobility; τ represents the dislocation line energy, $\tau = 0.5\mu b^2$; l is the mean free path of dislocation, which can be thought as the diameter of sub-grain, $l = 10\mu b/\sigma$.

The DRX nucleation rate $\dot{N}$ at temperature T can be represents as (Ref 14):

$$\dot{N} = N_c\dot{\varepsilon}\,\exp -\left(\frac{Q}{RT}\right) \qquad \text{(Eq 4)}$$

where N_c is nucleation rate constant.

2.2.3 Modeling of Grain Growth. The initial dislocation densities in the R-grain are almost zero after DRX. The deviation between the R-grain and the primary grain gives the driving force for the grain growth. The driving force is the stored strain energy. A grain boundary moves with a velocity (v) in response to the net pressure (f) on the boundary. It is generally assumed that the velocity is directly proportional to the pressure and that the constant of proportionality is the mobility (m) of the boundary as follows (Ref 4):

$$v = mf = \frac{b\delta D_{0b}}{kT}\exp\left(-\frac{Q}{RT}\right)\cdot f \qquad \text{(Eq 5)}$$

where δ is the characteristic grain boundary thickness, D_{0b} denotes the boundary self-diffusion coefficient, k represents the Boltzmaneural network's constant, $k = 1.381 \times 10^{-23}$ J K^{-1}.

In this study, it is assumed that the DRX grain is sphere. The driving force, f_i, for the growth of a grain of a radius, r_i, can then be expressed as

$$f_i = \tau(\rho_m - \rho_i) - 2\gamma_i/r_i \qquad \text{(Eq 6)}$$

where ρ_i and ρ_m are the dislocation density of i-grain and its surrounding deformed matrix, respectively, and γ_i is the grain boundary energy, which depends on the misorientation θ_i between the i-grain and its surrounding matrix as (Ref 13):

$$\gamma_i = \begin{cases} \gamma_m\frac{\theta_i}{\theta_m}\left(1 - \ln\frac{\theta_i}{\theta_m}\right), & \theta_i < 15^\circ \\ \gamma_m, & \theta_i \geq 15^\circ \end{cases} \qquad \text{(Eq 7)}$$

where θ_m and γ_m are the misorientation and the boundary energy for a high angle boundary, respectively.

3. High-Temperature Compression Testing

The experiments were carried out on AZ31 magnesium alloy with chemical compositions 3.2 Al, 0.8 Zn, and a minimum Mn content of 0.4 (wt.%). Hot-extruded AZ31 alloy bars of 47.2 mm in diameter were used in this study.

Cylindrical specimens of 10 mm in diameter and 12 mm in height were machined from hot-extruded bars with the axis along the extrusion direction. Compression tests were carried out at constant strain rates, such as 0.03, 0.3, 3, 30, and 90 s^{-1}, and temperature such as 300, 350, 400, 450, and 500 °C using Gleeble 3500. The specimen was resistance-heated through a thermocouple sending feedback signals to control the AC-current. In the present study, a very fine, fast-response thermocouple with a diameter of 0.08 mm was used for capturing the temperature changes occurring during the tests. Before deformation was initiated, graphite foils were put on the specimen's flat ends as lubricant. Specimens were preheated to the required temperature with a heating rate of 10 °C s^{-1} and homogenized for 60 s, then compressed to 4.4 mm in height, achieving a true strain of 1.0. All the tests were performed in a nitrogen atmosphere.

4. Inverse Identification of the Model Parameters

The inverse problem is typically referred to the determination of unknown model parameters in the direct problem. The accurate identification of the model parameters determines the reliable ones among the simulation results. In the CA model, the values of material parameters such as μ, b, and λ_m can be obtained from the literature or manuals. Other parameters, such as the initial hardening parameters h_0, initial recovery parameters r_0, and nucleation parameters, can be hardly determined form the experiments. The microstructure evolution during DRX will influence the flow stress of the material, which is easy to be obtained and relative reliable. Therefore, it is possible to identify the DRX parameters with inverse method, based on the measured flow stress.

The inverse method of solving process for the DRX parameters is shown in Fig. 1. It includes the following: (i) normalizing of input/output data containing the h_0, r_0, ρ_c, N_c, and a set of simulated flow stresses with strain using FEM; (ii) training BP network; (iii) initialing the DRX parameters at random, and predicting the flow stress by the BP network; (iv) comparing the predicted flow stress and the measured flow stress with strain; (v) putting the above DRX parameters into the first population, and calculating the new population by GA; (vi) adjusting the input parameters according the new population; and (vii) predicting the new stress by the BP network again to obtain the improved parameters, and (vii) recognizing the DRX parameters by repeating the above seven processes. The detail of each part of this process will be given in the following sections.

4.1 Training Data Samples Using Neural Networks

BP neural network is referred to as a type of computational models, which consists of hidden-layer neurons between the input and output neurons. The nonlinear hyperbolic functions are usually used as the activation functions to increase the modeling flexibility (Ref 19). In this study, the two-hidden layer BP neural network was adopted.

The samples for the training of the BP neural network model consist of a number of sets of inputs and outputs. First, in order to describe the inverse characteristics of AZ31 magnesium DRX parameters, these training samples including both the initial training and the retraining should be carefully selected. Then, these training samples should cover all possible values. In this study, the training samples were obtained by using finite-element method instead of carrying out an actual experiment.

For more stable and faster results, the stress was calculated for every true strain 0.1. Then, the true stress was obtained for every true strain 0.1 through compression tests by Gleeble 3500. The flow stress distribution was obtained using a commercial finite-element package, DEFORM to obtain the training samples; DEFORM was chosen as the platform for the numerical simulation operation because it has the ability to develop user-programmable routines to describe dependent boundary conditions spatially and temporally.

Second, for successfully utilizing BP neural network model, the inputs of the BP neural network model should be carefully chosen so that the variation in the outputs can be truthfully reflected by the changes of these inputs. Therefore, the DRX parameters of h_0, r_0, ρ_c, N_c are selected as the inputs.

It is well known that the flow stress changes are chiefly affected by two stages, which are dynamic recovery and DRX. In the BP neural network model, the stresses at every 0.1 strain were expressed as $y_1, y_2, \ldots, y_{10}$, respectively, and were used as the outputs for the BP neural network model, expressed as y in Fig. 3. Moreover, the 4-23-25-10 neural network is acquired after repeating calculation, and the global error is 0.025289.

According to Ref 27, the searching scopes of the DRX parameters are set as given in Table 1.

In this study, we construct orthogonal designs suitable for the study samples of neural network (Ref 27, 28). As there are four DRX parameters, an experimental design with four factors and nine levels will be denoted by orthogonal table $L_{32}(4^9)$, i.e., there are 32 sets of experiments. Then, the simulation flow stresses are acquired under certain temperature and strain rate. In addition, the study sample dates must be normalized between 0 and 1 before neural network training.

4.2 Optimization Using GA Model

Genetic algorithm (GA) is an important stochastic search algorithm for solving optimization problems based on the concept of natural selection and evolution processes (Ref 29, 30).

In this study, according to the characteristic of inverse method, the cost function can be defined as

$$E(\lambda) = \frac{1}{N}\sum_{i=1}^{N}\left(\frac{\sigma_i^* - \sigma_i^c}{\sigma_i^*}\right)^2 \quad \text{(Eq 8)}$$

where σ_i^c and σ_i^* are, respectively, neural network-calculated and test-measured flow stresses at the strains $\varepsilon_i (i = 1, \ldots, N)$; and N is the number of sample points on the stress-strain curve.

GA operates on a population of the parameters λ that are initially generated at random. The $E(\lambda)$ is set as the fitness for the individuals. GA seeks to attain the optimum value of the population by selecting the fittest individuals from the population and using their "genetic" information in "mating" operations to create a new population of solution.

Then, the input parameters λ are changed according the new population, and the new stress values are predicted by the BP neural network again as shown in Fig. 1. Repeat the above processes, until the rational parameters are found λ to satisfy the target function $E(\lambda) \leq 0.001$. In this study, after repeating calculations, the parameter values used in GA are as follows: population size $M = 50$, generation number $T = 300$, crossover probability $P_c = 0.7$, and mutation probability $P_m = 0.001$.

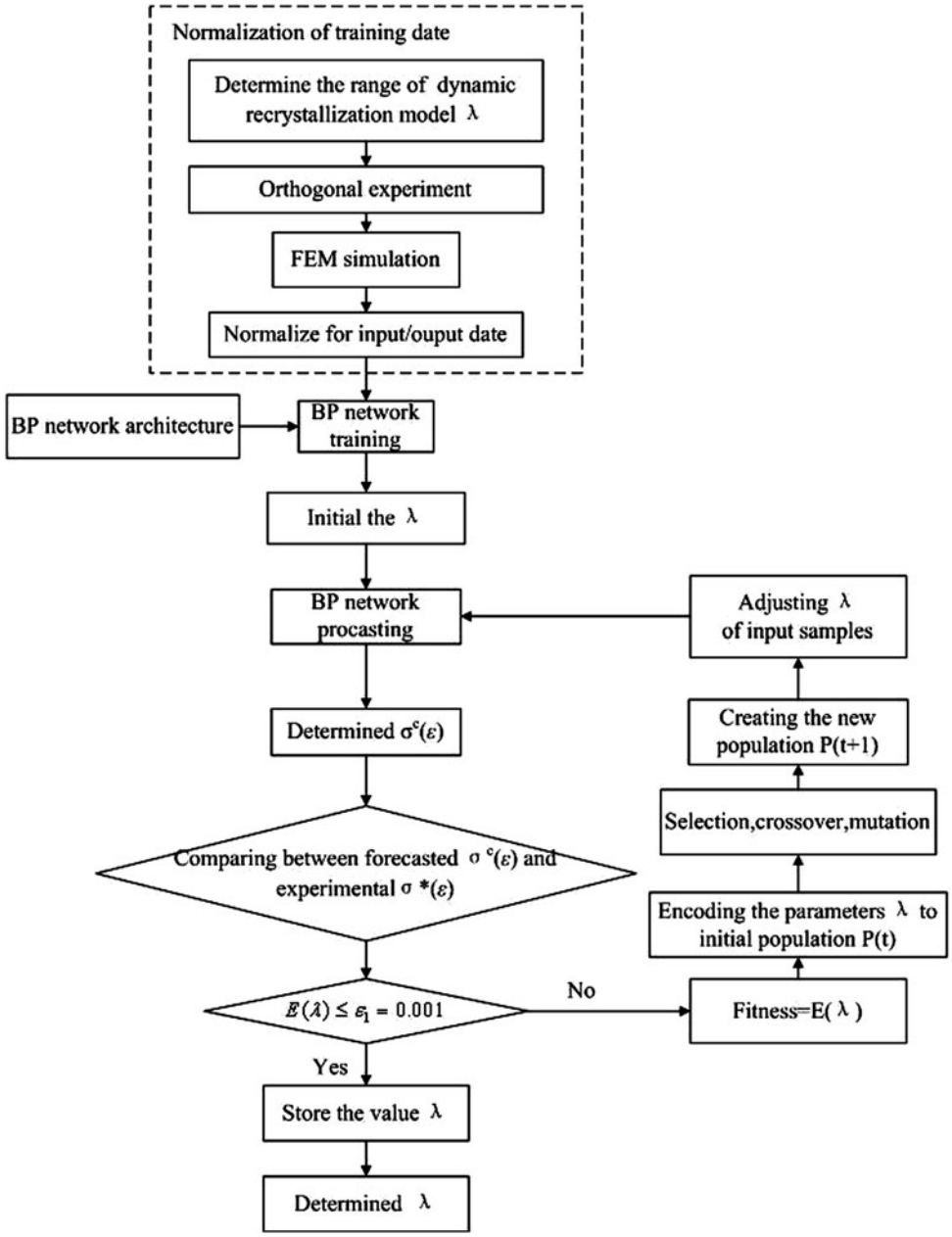

Fig. 1 Flow chart of inverse analysis algorithm using BP neural network and GA

Table 1 Parameters scopes

Parameter	Scopes
Critical dislocation density, m^{-2}	$\rho_c \in \{1.2809 \times 10^{14},\ 1.4976 \times 10^{14}\}$
Nucleation rate constant, $m^{-1}\ s^{-1}$	$N_c \in \{5000,\ 250000\}$
Initial work hardening	$h_0 \in \{1.0000 \times 10^{15},\ 1.2900 \times 10^{15}\}$
Initial dynamic recovery	$r_0 \in \{6.000,\ 8.900\}$

Moreover, to evaluate the effect of rate of deformation on the deformation behavior of the material at three specific temperatures, three different forming speeds are required under isothermal conditions in this study. Therefore, the cost function consists of nine terms as defined in Eq 9, namely, differences between the experimental and the corresponding flow stresses by BP network predicting in a least-square sense at three different forming velocities V_1, V_2, and V_3.

$$E(\lambda) = \sqrt{\frac{1}{3}\sum_{i=1}^{3}\left[\frac{1}{N}\sum_{j=1}^{N}\left(\frac{\sigma_{ij}^{*}-\sigma_{ij}^{c}}{\sigma_{ij}^{*}}\right)^{2}\right]}\Bigg|_{T_1} + \sqrt{\frac{1}{3}\sum_{i=1}^{3}\left[\frac{1}{N}\sum_{j=1}^{N}\left(\frac{\sigma_{ij}^{*}-\sigma_{ij}^{c}}{\sigma_{ij}^{*}}\right)^{2}\right]}\Bigg|_{T_2} + \sqrt{\frac{1}{3}\sum_{i=1}^{3}\left[\frac{1}{N}\sum_{j=1}^{N}\left(\frac{\sigma_{ij}^{*}-\sigma_{ij}^{c}}{\sigma_{ij}^{*}}\right)^{2}\right]}\Bigg|_{T_3} \quad \text{(Eq 9)}$$

Table 2 Parameters used in the simulations

Temperature, K	Q, kJ mol^{-1}	D_{0b}, m^3 s^{-1}	b, m	μ, Pa	γ_m, J m^{-2}
573	40	5.3×10^{-13}	3.21×10^{-10}	16.67×10^{10}	0.93
623	69				
673	113				

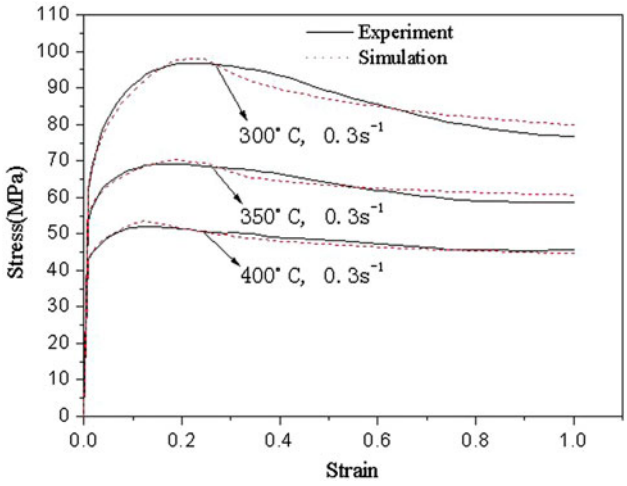

Fig. 2 Comparison between simulation and real stress

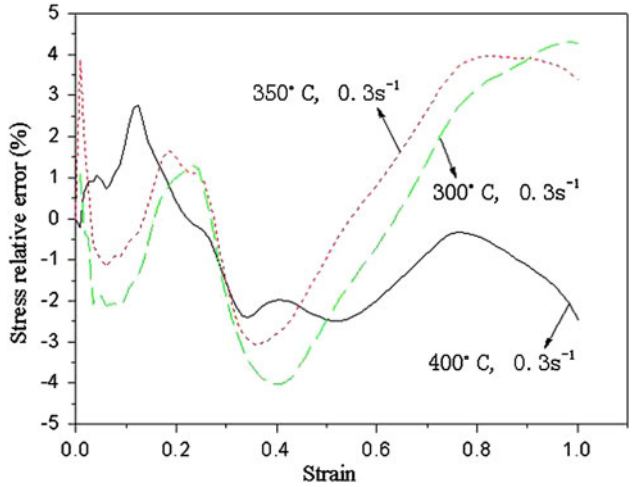

Fig. 3 Relative error of simulation stress

5. Simulation Results and Discussions

To verify the reliability of the identification method, three typical deformation processes were simulated. The simulation results of both the microstructure and the flow stress were compared with experimental measurements. Parameters used in the simulations are shown in Table 2 (Ref 31, 32).

In this study, the learn rate in the BP network is set as 0.05. By calculating with the developed inverse method, the optimum value of DRX parameters is identified as follows:

$$\rho_c = 1.340 \times 10^{14}\,\mathrm{m}^{-2}, \quad N_c = 1.295 \times 10^{4}\,\mathrm{m}^{-1}\,\mathrm{s}^{-1},$$

$$h_0 = 1.201 \times 10^{15}, \quad r_0 = 7.943.$$

5.1 Simulation Result of Flow Stress

Figure 2 shows the comparison between the predicted and measured flow stress. It can be found that the simulation results are generally in good agreement with experimental ones. According to Fig. 3, the maximum relative error of the simulated flow stress is about 5-8%.

The error of the simulation results are mainly caused by the developed inverse model. In the developed inverse model, it was assumed that when the dislocation density exceeds the critical value, the nucleation rate of DRX is a constant. However, actually, with the increasing deformation, the stored energy will increase, leading to the increasing of nucleation rate. If the nucleation rate was set as a constant, then the set value will be greater than the real nucleation rate at the start of DRX, and less than the real nucleation rate at the steady stage, which can be corresponded to the discrepancy between the simulated and measured flow stresses shown in Fig. 2.

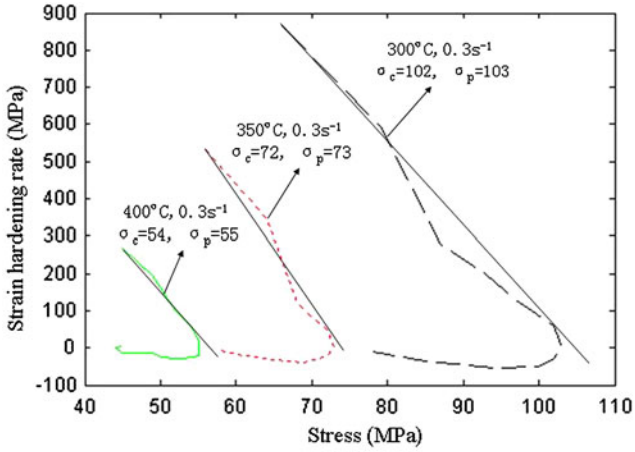

Fig. 4 Hardening rate curve

Figure 4 shows the simulated strain hardening rate $\theta(\theta = d\sigma/d\varepsilon)$. It can be seen that strain hardening rate is high at the initial stage, indicating that work hardening is the dominant mechanism. Then, it decreases rapidly. When the temperature and strain rates meet certain conditions, DRX occurs. When the stress reaches a critical value, then the critical strain can be obtained accordingly.

Figure 5 shows that the peak strains ε_p at different temperatures are close to the measured values, and the ratios of the simulated critical strain to peak strain $(\varepsilon_c/\varepsilon_p)$ are between 0.64 to 0.83, being in very good agreement with the theoretical values in the range of 0.65-0.90.

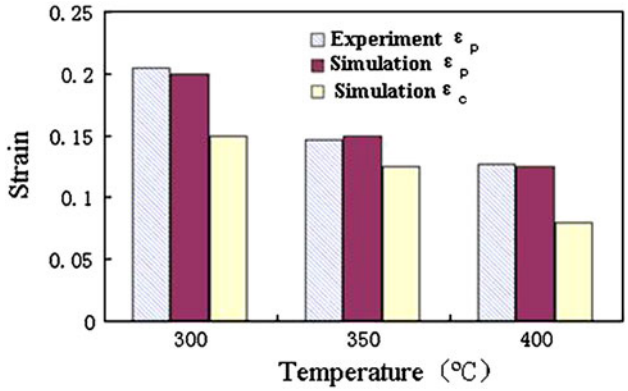

Fig. 5 Comparison between the true peak strain, simulation peak strain, and critical simulation strain

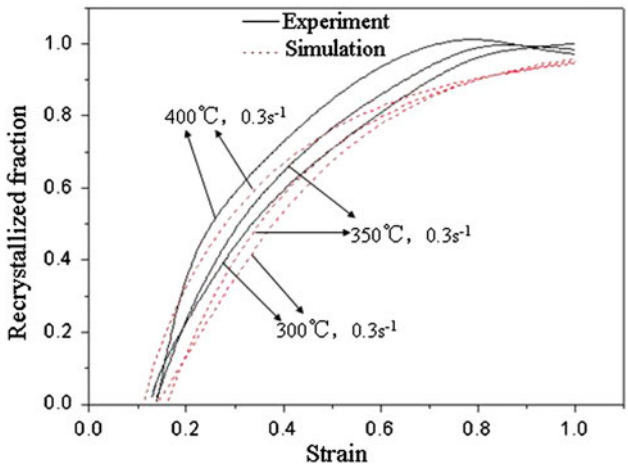

Fig. 6 Comparison between the simulation and experimental fractions of dynamic recrystallization at different temperature

5.2 Simulation Results of Microstructure Evolution

The CA method deals with an array of cell, the evolution of which is characterized by the state of cell determined by the neighborhood and the transformation rule. For the purpose of simulating the DRX behavior, the simulation space is disintegrated into an array of equally shaped quadratic cells of 80 × 80 sites with the periodic boundary conditions. The size of each lattice site is 1 μm, and the simulation lattice represents 80 μm × 80 μm in the real material.

Figure 6 shows the fraction of DRX during deformation of AZ31 magnesium alloy. It can be found that the initialization strain for DRX is about 0.15. The volume fraction of DRX increases with the increasing of strain. In addition, the volume fraction of DRX also increases with the increasing deformation temperature. However, when the strain reaches 0.9, the volume fractions of DRX are similar at different temperatures. From Fig. 6, it can also be found that the error between the calculated and the measured volume fractions of DRX is less than 9%. The DRX volume fractions of the compressed samples were measured using a TSL EBSD system (SIT camera, OIMTM 4 software) attached to a Zeiss Gemini 982DSM (primary electron energy: 20 keV; probe current: 2.8 nA).

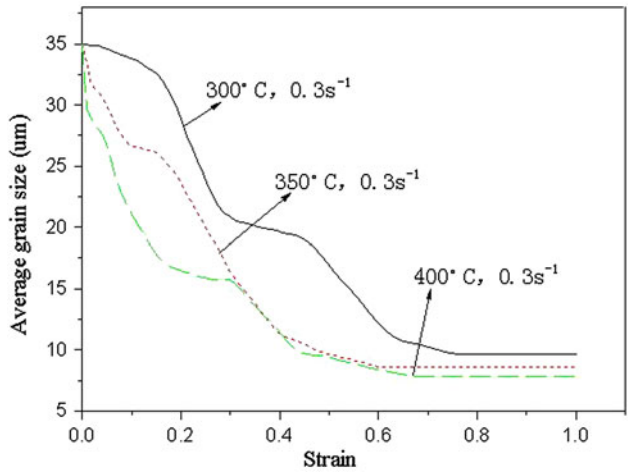

Fig. 7 Change of simulation average grain size with strain

Figure 7 shows the quantitative description of the microstructure evolution during hot deformation process. It can be seen that the grain size decreases with the deformation strain. For example, at the temperature of 400 °C, the grain size decreases from 35 μm to about 5 μm.

Figure 8 shows the comparison between the simulated and measured grain structures of the compressed samples. The observational face was taken along the axial direction of the deformed specimens, then ground, and polished, followed by etching with Acetic-Picric acid (4.2 vol.%). The metallographic analysis was carried out on DM1500 instrument. The mean grain size of microstructure was taken to be the average value of 20 fields of view. In Fig. 8, it is seen that a close agreement between the experimental measurements and computed ones was achieved. At the strain of 0.2, serration and bulges develop, and eventually new grains are generated along the primary grain boundaries, leading to a beck lace structure. The average grain size is about 16.98 μm. At the strain of 0.5, most of the primary grains are recrystallized. The average grain size is about 9.05 μm. When the strain reaches 1.0, the structure is fully recrystallized. Homogeneous distribution of fine equiaxed grain structure is obtained. The average grain size is about 5.72 μm.

6. Conclusions

(1) The AZ31 DRX model parameters have been successfully determined by using the method of inverse analysis based on measured stress at every 0.1 true strain, BP neural network algorithm, genetic algorithm, orthogonal experiment, and numerical simulation.

(2) The correctness of method has been verified through the comparison between the numerically calculated and the compressed experimental results based on the identified parameters used in finite element analysis. The results show that the numerically calculated stresses, strains, recrystallized fractions, and average grain sizes are in very good agreement with the experimental ones. It is satisfactorily demonstrated that the method of inverse analysis is a feasible and an effective tool for the determination of the AZ31 DRX model parameters.

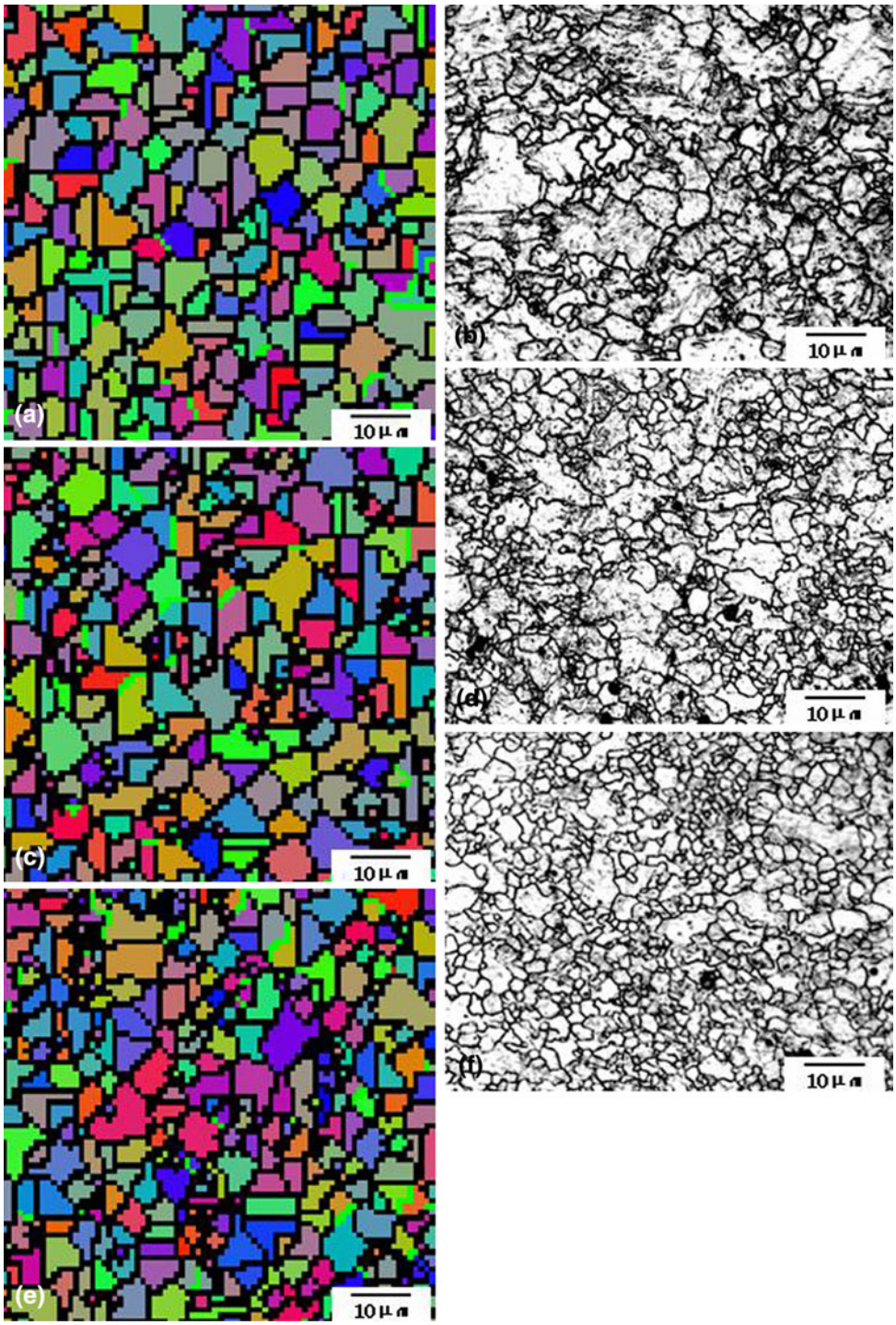

Fig. 8 Comparison between the simulated and measured grain structures (400 °C, 0.3 s^{-1}). (a) ε = 0.2 (FEM simulation), (b) ε = 0.2 (experiment), (c) ε = 0.5 (FEM simulation), (d) ε = 0.5 (experiment), (e) ε = 1 (FEM simulation), and (f) ε = 1 (experiment)

Acknowledgments

The authors acknowledge gratefully the financial supports received from the National Science Foundation (No. 51075132), and the Science Fund of State Key Laboratory of Advanced Design and Manufacturing for Vehicle Body (No. 30815007).

References

1. J.W. Liu, D. Chen, Z.H. Chen, and H.G. Yan, Deformation Behavior of AZ31 Magnesium Alloy During Tension at Moderate Temperatures, *J. Mater. Eng. Perform.*, 2009, **18**(7), p 966–972
2. J. Liu, Z. Cui, and C. Li, Modelling of Flow Stress Characterizing Dynamic Recrystallization for Magnesium Alloy AZ31B, *Comput. Mater. Sci.*, 2008, **41**, p 375–382

3. A. Galiyev, R. Kaibyshev, and G. Gottstein, Correlation of Plastic Deformation and Dynamic Recrystallization in Magnesium Alloy ZK60, *Acta Mater.*, 2001, **49**, p 1199–1207
4. Y. Zhang, X. Zeng, C. Lu, and W. Ding, Deformation Behavior and Dynamic Recrystallization of a Mg-Zn-Y-Zr Alloy, *Mater. Sci. Eng. A*, 2006, **428**, p 91–99
5. X. Zhao, K. Zhang, X. Li et al., Deformation Behavior and Dynamic Recrystallization of Mg-Y-Nd-Gd-Zr Alloy, *J Rare Earths*, 2008, **26**(6), p 846–850
6. T. Al-Samman and G. Gottetein, Dynamic Recrystallization During High Temperature Deformation of Magnesium, *Mater. Sci. Eng. A*, 2008, **490**, p 411–420
7. S. Huang, Y. Yi, and C. Liu, Simulation of Dynamic Recrystallization for Aluminium Alloy 7050 Using Cellular Automation, *J. Cent. South Univ. Technol.*, 2009, **16**, p 18–24
8. A.D. Rollet and D. Raabe, A Hybrid Model for Mesoscopic Simulation of Recrystallization, *Comput. Mater. Sci.*, 2001, **21**, p 69–78
9. C.H.J. Davies, Growth of Nuclei in a Cellular Automation Simulation of Recrystallization, *Scripta Mater.*, 1997, **36**, p 35–40
10. N. Yazdipour, C.H.J. Davies, and P.D. Hodgson, Microstructural Modeling of Dynamic Recrystallization Using Irregular Cellular Automata, *Comput. Mater. Sci.*, 2008, **44**, p 566–576
11. Z.-y. Jin, J. Liu, Z.-s. Cui, and D.-l. Wei, Identification of Nucleation Parameter for Cellular Automation Model of Dynamic Recrystallization, *Trans. Nonferrous Met. Soc. China*, 2010, **20**, p 458–464
12. H. Xiao and H.B. Xie, Simulation of Dynamic Recrystallization Using Cellular Automaton Method, *J. Iron Steel Res.*, 2004, **11**(2), p 42–45
13. S. Ghosh, P. Gabane, A. Bose, and N. Chakraborti, Modeling of Recrystallization in Cold Rolled Copper Using Inverse Cellular Automata and Genetic Algorithm, *Comput. Mater. Sci.*, 2009, **45**, p 96–103
14. X.G. Fan, H. Yang, Z.C. Sun, and D.W. Zhang, Quantitative Analysis of Dynamic Recrystallization Behavior Using a Grain Boundary Evolution Based Kinetic Model, *Mater. Sci. Eng. A*, 2010, **527**, p 5368–5377
15. J. Kusiak, R. Kawalla, M. Pietrzyk, and H. Pircher, Inverse Analysis Applied to the Evaluation of Material Parameters in the History Dependent Flow Stress Equation in Hot Forming of Metals, *J. Mater. Process. Technol.*, 1996, **60**, p 455–461
16. R. Forestier, E. Massoni, and Y. Chastel, Estimation of Constitutive Parameters Using an Inverse Method Coupled to a 3D Finite Element Software, *J. Mater. Process. Technol.*, 2002, **125–126**, p 594–601
17. Z.-C. Lin, C.-C. Chen, and H.-H. Wang, The Determination of Material Strength Coefficient and Strain Hardening Constant by Inverse Method, *J. Mater. Process. Technol.*, 2009, **209**, p 2393–2401
18. Z. Jin and Z. Cui, Investigation on Strain Dependence of Dynamic Recrystallization Behavior Using an Inverse Analysis Method, *Mater. Sci. Eng. A*, 2010, **527**, p 3111–3119
19. L. Zhang, L. Li, H. Ju, and B. Zhu, Inverse Identification of Interfacial Heat Transfer Coefficient Between the Casting and Metal Mold Using Neural Network, *Energy Convers. Manag.*, 2010, **51**, p 1898–1904
20. N. Kim and H. Choi, The Prediction of Deformation Behavior and Interfacial Friction Under Hot Working Conditions Using Inverse Analysis, *J. Mater. Process. Technol.*, 2008, **208**, p 211–221
21. L.N. Smith, R.M. German, and M.L. Smith, A Neural Network Approach for Solution of the Inverse Problem for Selecting of Powder Metallurgy Materials, *J. Mater. Process. Technol.*, 2002, **120**, p 419–425
22. S. Deng and Y. Hwang, Applying Neural Networks to the Solution of Forward and Inverse Heat Conduction Problems, *Int. J. Heat Mass Transfer*, 2006, **49**, p 4732–4750
23. Y.C. Liang, D.P. Feng, G.R. Liu, X.W. Yang, and X. Han, Neural Identification of Rock Parameters Using Fuzzy Adaptive Learning Parameters, *Comput. Struct.*, 2003, **81**, p 2373–2382
24. N. Huber and Ch. Tsakmakis, A Neural Network Tool for Identifying the Material Parameters of a Finite Deformation Viscoplasticity Model, *Comput. Methods Appl. Mech. Eng.*, 2001, **191**, p 353–384
25. M. Qian and Z.X. Guo, Cellular Automata Simulation of Microstructural Evolution During Dynamic Recrystallization of an HY-100 Steel, *Mater. Sci. Eng. A*, 2004, **365**, p 180–185
26. H.W. Lee and Y.-T. Im, Numerical Modeling of Dynamic Recrystallization During Nonisothermal Hot Compression by Cellular Automata and Finite Element Analysis, *Int. J. Mech. Sci.*, 2010, **52**, p 1277–1289
27. S.D. Georigiou, Orthogonal Designs for Computer Experiments, *J. Stat. Plann. Infer.*, 2011, **141**, p 1519–1525
28. O.I. Adesola, Orthogonal Experiments in the Development of Carbon-Resin for Chloride Removal from Solutions, *Stat. Methodol.*, 2009, **6**(3), p 109–119
29. A.A. Javadi, R. Farmani, and T.P. Tan, A Hybrid Intelligent Genetic Algorithm, *Adv. Eng. Inform.*, 2005, **19**, p 255–262
30. S.-F. Hwang and R.-S. He, A Hybrid Real-Parameter Genetic Algorithm for Function Optimization, *Adv. Eng. Inform.*, 2006, **20**(1), p 7–21
31. Z. Jin, *Modeling and Simulation of Dynamic Recrystallization for Hot Deformed Low Carbon Steel by Inverse Analysis Method*, Shanghai Jiao Tong University, 2010
32. M. Kassner and M. Perez-Prado, Five-Power-Law Creep in Single Phase Metals and Alloys, *Prog. Mater. Sci.*, 2000, **45**, p 91–102